Origin of two-dimensional electronic states at Si- and Gd-terminated surfaces of GdRh$_2$Si$_2$(001)

A. Yu. Vyazovskaya [1,2,*] M. M. Otrokov,[3,4,5] Yu. M. Koroteev,[6,1,2] K. Kummer,[7]
M. Güttler,[8] D. V. Vyalikh,[5,4] and E. V. Chulkov[9,5,2,3]

[1]*Tomsk State University, Tomsk 634050, Russia*
[2]*St. Petersburg State University, St. Petersburg 198504, Russia*
[3]*Centro de Física de Materiales (CFM-MPC), Centro Mixto CSIC-UPV/EHU, 20018 Donostia-San Sebastián, Basque Country, Spain*
[4]*IKERBASQUE, Basque Foundation for Science, 48011 Bilbao, Basque Country, Spain*
[5]*Donostia International Physics Center (DIPC), 20018 Donostia-San Sebastián, Basque Country, Spain*
[6]*Institute of Strength Physics and Materials Science, Tomsk 634055, Russia*
[7]*European Synchrotron Radiation Facility, 71 Avenue des Martyrs, CS 40220, 38043 Grenoble Cedex 9, France*
[8]*Institute of Solid State Physics, Dresden University of Technology, D-01062 Dresden, Germany*
[9]*Departamento de Física de Materiales, Facultad de Ciencias Químicas, UPV/EHU, 20080 Donostia-San Sebastián, Basque Country, Spain*

We present a first-principles study of the GdRh$_2$Si$_2$(001) surface electronic structure. Two surfaces, Si- and Gd-terminated, are considered. The origin of the two-dimensional (2D) electronic states at both terminations is investigated by tracing the band structure evolution by going from individual Si, Rh, and Gd atomic layers to (non)stoichiometric ultrathin films and, finally, to thicker GdRh$_2$Si$_2$ slabs. We find the conic-like (Dirac-like) resonance state located in the vicinity of the $\overline{\Gamma}$ point at the Si termination to form via the Tamm mechanism and explain the reasons for the differences in dispersion and energy position of the resonance states at the Si and Gd terminations. Then, we show how the butterfly-like dispersion of the Shockley state, residing in the bulk projected band gap near the $\overline{M}$ point, appears due to the interaction of the bands localized in the surface and subsurface Gd-Si-Rh-Si blocks of the Si termination. Also, a giant sign-alternating atomic relaxation near both the Si- and Gd-terminated surfaces is revealed and its effect on the dispersion and energy position of the 2D states is discussed. In this way we shed light on the origin of the 2D states and explain their dispersion seen in angle-resolved photoemission spectroscopy experiments.

I. INTRODUCTION

The electronic structure and magnetic interactions in rare-earth intermetallic materials have permanently attracted wide attention due to their rich and unusual physical properties covering magnetism, superconductivity, valence fluctuations, heavy-fermion, and Kondo behavior [1–19]. The key role in these phenomena is played by the partially filled $4f$ shell that lies deep inside the ionic core and maintains, therefore, its localized atomic character and, notably, its magnetic moment in the solid state. Remarkably, the respective phenomena and in particular the magnetic properties near the surface appear to be essentially different from those in the bulk [20,21]. At present, the REX_2Si$_2$ systems, where RE is a rare-earth and X is a transition or noble metal element, of the ThCr$_2$Si$_2$-type structure are being intensively studied [20–35], in particular with the aim to disclose and elucidate those exotic properties near the surface [20,21,27,35–39] which are linked and handled via the interplay of $4f$ and itinerant states.

The ARPES experiments on the REX_2Si$_2$ systems suggest that their surface presents usually a kind of mosaic of Si- and RE-terminated crystallites whose size, however, allows finding and accurately exploring the electronic structure exclusively from each type of terminations. It has been established that the Si-terminated surfaces of such systems feature Shockley surface states located around the $\overline{M}$ point and resonance states near the $\overline{\Gamma}$ point [20,21,36–43]. The origin of the Shockley surface states is well known [44]. They arise in the local projected band gap of a metal or in the fundamental energy gap of semiconductors due to inversion of the band gap edges. The latter means a change of the order in which the orbitals appear at the edges of the inverted band gap with the increase of energy [45]. A classical example of Shockley states is the states at the noble metal (111) and (110) surfaces at the $\overline{\Gamma}$ [46,47] and $\overline{Y}$ points [48,49], as well as at the Be(0001) surface [50,51]. In REX_2Si$_2$, the Shockley surface states lie in the inverted bulk projected band gap at the $\overline{M}$ point, and in the real space they are localized in a few atomic layers near the Si-terminated surface [20,21,36].

A characteristic feature of the surface resonance states (hereinafter simply "resonance states"), which also demonstrate a high amplitude near the surface, is that they are located outside the bulk projected band gaps, thus hybridizing with the bulk states of the material. The resonant nature of the two-dimensional (2D) states in the vicinity of the $\overline{\Gamma}$ point at the REX_2Si$_2$(001) surface is convincingly demonstrated by recent photoemission measurements [38,40] and first-principles calculations [21].

*alex_vyaz93@mail.ru

In EuRh$_2$Si$_2$, GdRh$_2$Si$_2$, and YbCo$_2$Si$_2$, the resonance states at the $\overline{\Gamma}$ point reveal linear dispersion characteristic of the conic (Dirac) type of the electron spectrum [20,21,37,52]. It has been proposed in Ref. [21] that these resonant states can open an additional exchange channel that links the magnetic subsystems at the surface and in the bulk. In contrast to the Shockley surface states located inside the bulk projected band gap near the $\overline{M}$ point, the formation mechanism of the resonance state near the $\overline{\Gamma}$ point in compounds of the REX_2Si$_2$ type still remains unexplored.

In this paper, using first-principles electronic structure calculations, we study the origin of the 2D electronic states at the Si- and Gd-terminated surfaces of GdRh$_2$Si$_2$(001). We show that the surface resonance states at the Si termination at the $\overline{\Gamma}$ point appear via the Tamm mechanism [53]. They split off from the continuum of the projected bulk states of similar dispersion and the same orbital character into a so-called symmetry gap, i.e., in a region of the projected states of different symmetry with which they do not interact [45]. As the surface resonance states at the $\overline{\Gamma}$ point appear at both considered terminations, the reasons for the differences in their dispersion and energy positions are also discussed. We further explain in great detail the origin of the butterfly-like dispersion of the Shockley state, which is formed due to hybridization of the bands localized in the surface and sub-surface Gd-Si-Rh-Si 4-layer blocks of the Si termination. The other band involved in this hybridization forms an additional surface state lying deeper in energy, that should be seen in photoemission as well. We believe that the results obtained in this study reflect general electronic structure features of the (001) surfaces of a wide class of REX_2Si$_2$ compounds and elucidate the dispersion of surface and resonance states seen in ARPES experiments.

The paper is organized as follows. The computational details are presented in Sec. II. Section III A focuses on the structural properties of the bulk and both surface terminations of GdRh$_2$Si$_2$. In Sec. III B we introduce the 2D electronic features of GdRh$_2$Si$_2$(001) that we are interested in and describe briefly the effect of the spin-orbit and magnetic interactions. Then, in Secs. III C 1, III C 2, and III D we disclose the origin of all those features and discuss the dependence of their dispersion and energy position on the surface termination. Concluding remarks close the paper in Sec. IV.

II. METHOD AND CALCULATION DETAILS

GdRh$_2$Si$_2$ crystallizes in the tetragonal body-centered ThCr$_2$Si$_2$-type structure, characterized by space group $I4/mmm$ [54]. Its atomic crystal structure is completely determined by three parameters a, c, z_{Si}, where a and c describe a simple tetragonal lattice, and z_{Si} defines the positions of the Si atoms along the tetragonal axis as well as two interlayer spacings $d^0_{Gd-Si} = cz_{Si}$ and $d^0_{Si-Rh} = c(\frac{1}{4} - z_{Si})$. Regarding the magnetism of GdRh$_2$Si$_2$, the local moments in GdRh$_2$Si$_2$ are localized exclusively on the Gd ions [55]. Below the Néel temperature $T_N \sim 107$ K, each Gd layer is ordered ferromagnetically, while the ordering between the neighboring layers is antiferromagnetic [56] [see Fig. 1(a)]. The calculations of the GdRh$_2$Si$_2$ antiferromagnetic phase were performed for two orientations of the Gd $4f$ moments, i.e., parallel to [110]
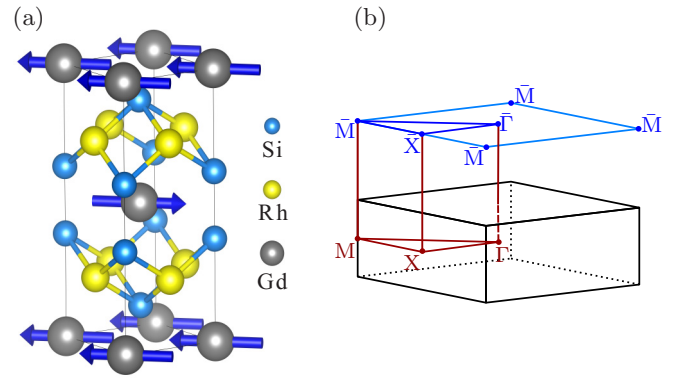
FIG. 1. (a) Crystal and magnetic structures of GdRh$_2$Si$_2$. Blue arrows indicate the orientation of the magnetic moments in the Gd layers. The interlayer antiferromagnetic order reduces the symmetry to $P4/mmm$. (b) Bulk (black) and surface (blue) Brillouin zone for antiferromagnetic GdRh$_2$Si$_2$.

and [100], in order to assess the sensitivity of the electronic structure to the local moment orientation. The choice of these directions is caused by the experimental observations that, first, the Gd moments are locked within the GdRh$_2$Si$_2$ basal plane and, second, the basal plane magnetic anisotropy is weak [57].

The calculations were performed within density functional theory (DFT) using the projector augmented wave method (PAW) [58] implemented in the VASP code [59,60] and the full-potential linearized augmented plane wave method (FLAPW) [61], implemented in the FLEUR program package [62]. To describe the exchange-correlation energy, we used the generalized gradient approximation in the Perdew-Burke-Ernzerhof form [63]. Scalar-relativistic corrections were included in the Hamiltonian, and the spin-orbit interaction was taken into account by the second variation method [64]. To describe the Gd $4f$ and Rh $4d$ states, we used the GGA+U approach [65,66]. The values $U = 6.7$ eV, $J = 0.7$ eV and $U = 3.5$ eV, $J = 0.6$ eV were used for the Gd $4f$ and Rh $4d$ states, respectively [21]. The Brillouin zone was sampled with a $12 \times 12 \times 4$ and $12 \times 12 \times 1$ **k**-point grid in the case of the bulk and slab calculation, respectively. Bulk atomic structure optimization was carried out by finding the total energy minimum as a function of the a, c, and z_{Si} parameters. In the film geometry, all atomic layers were allowed to shift upon relaxation. All structural optimizations were performed using a force tolerance criterion for convergence of 10 meV/Å. The charge transfer was analyzed using the Bader method [67].

In the PAW calculations, a basis set of plane waves with energies up to 400 eV was used. The surface electronic structure was calculated by using a thick-film model for two different cases, where the Gd $4f$ electrons were treated either as valence or as core electrons. For the thin-film band structure calculations, that were used to study the origin of the 2D states of interest, the Gd $4f$ electrons were placed in the core. This does not affect the conclusions made since, when included in the valence band, the $4f$ states are located well below and above the Fermi level and therefore do not hybridize with the states that we are interested in.

TABLE I. Relaxed interlayer spacings d_{ij} and the relative relaxation $\Delta d_{ij}/d_{ij}^0$ for the Si- and Gd-terminated GdRh$_2$Si$_2$(001) surfaces. The subscripts i and j number the layers of the film, starting with the surface layer, and L denotes the sort of the atoms that form the layer. Relative relaxations smaller than 0.03% are not shown.

Si-terminated surface			Gd-terminated surface		
L_i - L_j	d_{ij} (Å)	$\Delta d_{ij}/d_{ij}^0$ (%)	L_i - L_j	d_{ij} (Å)	$\Delta d_{ij}/d_{ij}^0$ (%)
Si$_1$–Rh$_2$	1.152	−9.80	Gd$_1$–Si$_2$	0.966	−22.29
Rh$_2$–Si$_3$	1.226	−3.93	Si$_2$–Rh$_3$	1.345	5.39
Si$_3$–Gd$_4$	1.305	4.94	Rh$_3$–Si$_4$	1.324	2.22
Gd$_4$–Si$_5$	1.193	−3.99	Si$_4$–Gd$_5$	1.188	−2.95
Si$_5$–Rh$_6$	1.295	1.50	Gd$_5$–Si$_6$	1.286	3.45
Rh$_6$–Si$_7$	1.288	0.92	Si$_6$–Rh$_7$	1.277	0.03
Si$_7$–Gd$_8$	1.228	−1.22			
Gd$_8$–Si$_9$	1.261	1.47			
Si$_9$–Rh$_{10}$	1.278	0.16			
Rh$_{10}$–Si$_{11}$	1.277	0.03			

In the calculations by the FLAPW method, the core states were treated fully relativistically, while the valence states were calculated both in the scalar-relativistic approximation and taking into account spin-orbit interaction. The radii of the Gd, Rh, and Si muffin-tin spheres (R_{MT}) were set to 3.0, 2.3, and 2.0 a.u., respectively. The value of the cutoff parameter of the plane wave basis $k_{max} = 4.0$ a.u.$^{-1}$ corresponded to ~150 basis functions per atom.

The GdRh$_2$Si$_2$(001) surface was simulated by an asymmetric 32-layer film with Gd- and Si-terminated surfaces. The bulk crystal structure parameters and the interlayer spacings in the 32-layer film were optimized using the FLAPW method. The calculations of the electronic band structure were carried out within both the PAW and FLAPW methods. The electronic band structures obtained within these methods are found to be in good agreement with each other. To study the origin of the surface and resonance states, electronic structure calculations for 4-, 8-, 12-, 16-, and 20-layer-thick films of GdRh$_2$Si$_2$ as well as for 3-layer Si-Rh-Si films were carried out in the framework of the PAW method.

III. RESULTS AND DISCUSSION

A. Bulk and surface atomic structure

Bulk atomic structure optimization yields the lattice parameters $a = 4.066$ Å and $c = 10.078$ Å, which are by 0.6% and 0.92% larger than the corresponding experimental values [56], and $z_{Si} = 0.123$. These parameters lead to the bulk interlayer spacings $d_{Gd-Si}^0 = 1.243$ Å, $d_{Si-Rh}^0 = 1.276$ Å, which correspond to the Si-Gd and Si-Rh bond lengths of 3.133 Å and 2.400 Å, respectively.

The optimization of the interlayer distances d_{ij} in the 32-layer film revealed a gigantic sign-alternating relaxation near both the Si and Gd surfaces. The calculated d_{ij} as well as the relative relaxations near the surfaces $\Delta d_{ij}/d_{ij}^0$ are given in Table I. Here, $\Delta d_{ij} = d_{ij} - d_{ij}^0$, and d_{ij}^0 stands for the bulk interlayer distances given above. It can be seen that at the Si-terminated surface the relaxation penetrates very deeply

into the film (up to 11 layers). The outermost 3-layer Si-Rh-Si block is compressed by 6.84%, while the second 3-layer expands by 1.21%. The relaxations in the third 3-layer are very small and its thickness is only by 0.12% larger than in the bulk. We also note that, as a result of the relaxation, the spacings between the Si and Rh layers in each single 3-layer Si-Rh-Si block are relaxed in the same way; i.e., they both either increase or decrease together. The adjacent interlayer spacings Si-Gd and Gd-Si exhibit relative relaxation of opposite signs: if one of them contracts, the other increases, and vice versa.

At the Gd surface, the relaxation penetrates up to 7 layers into the film. The thickness of the outermost (second) 3-layer Si-Rh-Si block appears to be increased by 4.60% (0.04%; i.e., the second 3-layer is practically bulk-like). Just as at the Si-terminated surface, at the Gd-terminated surface the sign-alternating relaxation of the adjacent interlayer spacings Si-Gd and Gd-Si is also observed.

Thus, a compression of the topmost interlayer spacing and rather complicated relaxation of the deeper layers are seen at the GdRh$_2$Si$_2$(001) surface irrespective of its termination. This indicates a significant redistribution of the valence electron density of the compound near both the Si- and Gd-terminated surfaces.

B. Electronic structure of the GdRh$_2$Si$_2$(001) surface

Figure 2 shows the calculated 2D electronic states at both the Si- [Figs. 2(a), 2(c)] and Gd-terminated [Figs. 2(b), 2(d)] surfaces of the 32-layer GdRh$_2$Si$_2$(001) film, as well as the bulk projected bands. For the paramagnetic state [Fig. 2(a), 2(b)], the electronic structure calculations were carried out in the scalar-relativistic approximation. For the antiferromagnetic state [Fig. 2(c), 2(d)], the spin-orbit interaction was also taken into account. In the latter case the alignment of the Gd 4f moments along the [110] direction was considered. Orange and green circles mark the bands localized in the outermost four atomic layers (4-layer block) of the Si and Gd surfaces, respectively, while blue circles highlight the bands localized in the subsurface 4-layer block of the Si termination. The reason for displaying the contributions of the second 4-layer block of the Si termination is the participation of the corresponding bands in formation of the characteristic butterfly-like shape of the Shockley surface state along the $\overline{X}$–$\overline{M}$–$\overline{X}$ direction, as will be shown below.

Let us first discuss the surface electronic structures calculated with no spin-orbit interaction and magnetism included. At the Si termination, surface and resonance states are observed along all high-symmetry directions of the surface Brillouin zone (SBZ) [Fig. 1(b)], as can be seen in Fig. 2(a). Near the $\overline{\Gamma}$ point, two electron-like and two hole-like bands are seen (i.e., one orange and one blue band of each type). The electron-like (hole-like) pair of bands is labeled as α (β). By attributing a single label to a pair of bands we emphasize their similar origin as it is clarified further. Both α and β bands are created mainly by the d_{xy} orbitals of the Rh$_2$ (orange) and Rh$_6$ (blue) layers, respectively (here the atomic layers are numbered as in Table I). The differences of dispersions within each pair are caused by the different localization and structural relaxations (see Sec. III D). The orange band of the
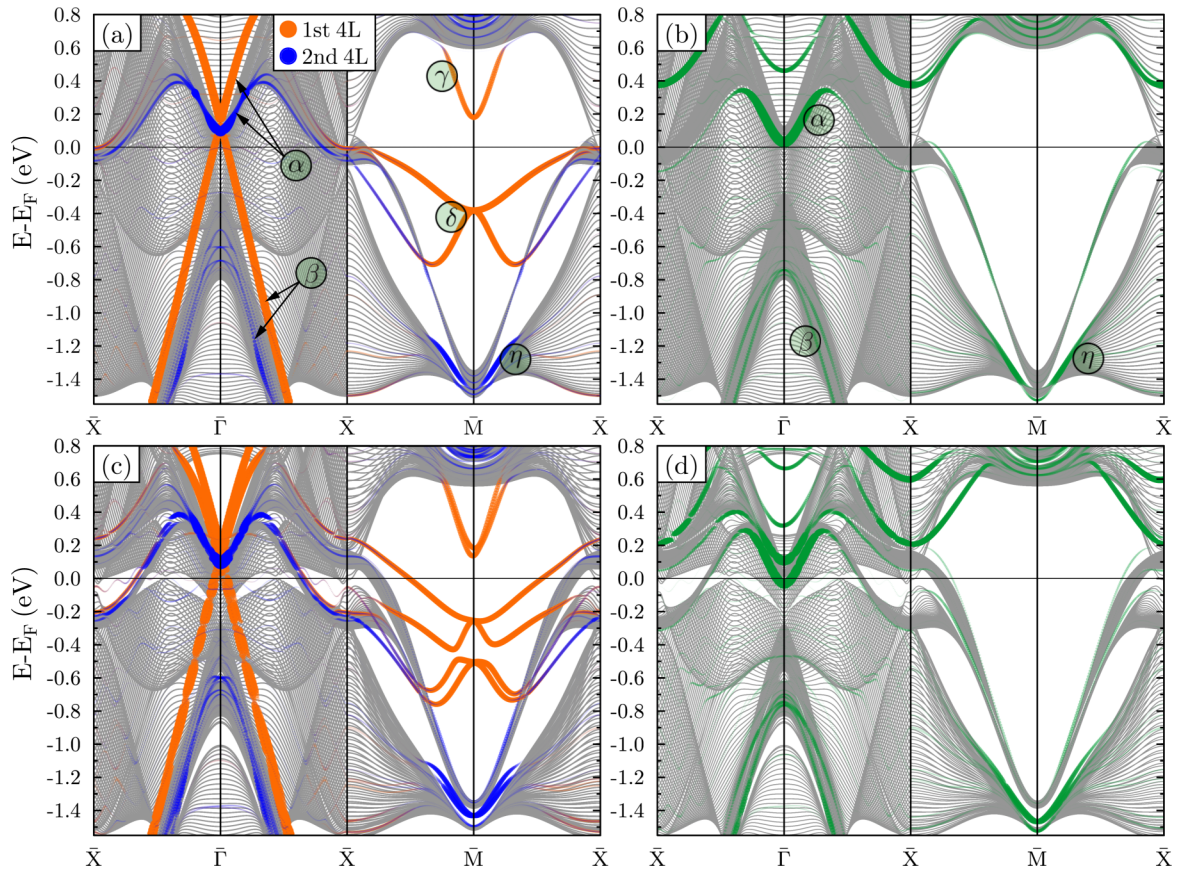
FIG. 2. Surface band structure of GdRh$_2$Si$_2$ calculated along the high-symmetry directions of the SBZ for the surfaces terminated by Si [(a), (c)] and Gd [(b), (d)] layers. The calculations were performed for the 32-layer film both without including the spin-orbit and magnetic interactions [(a), (b)] and taking them into account [(c), (d)]. Orange and blue symbols show the 2D electronic states, located in the outermost and second 4-layer (4L) blocks of the Si termination, respectively, while green symbols mark the states of the outermost 4-layer block of the Gd termination. The size of the color circle reflects the weight of the state in the particular 4-layer block. Bulk projected bands are shown in gray.

β pair, characterized by a linear dispersion, is the resonance state seen in the photoemission experiment [21]. The bands of the α pair are located in the conduction band and therefore are not seen in ordinary photoemission, that probes only occupied states. As we will show below, at the Si termination these states are formed via the Tamm mechanism [68], that suggests the 2D bands splitting off from the continuum of the bulk states of similar dispersion and the same orbital character into the symmetry gap.

Inside the projected bulk band gap in the vicinity of the $\overline{\text{M}}$ point, three Shockley surface states localized mainly in the outermost four atomic layers are observed [Fig. 2(a)]. The butterfly-shaped states (labeled as δ) lying below the Fermi level are built up mainly by the $d_{x^2-y^2}$ and d_{z^2} orbitals of the Rh$_2$ layer with an admixture of the p orbitals of the Si$_1$ and Si$_3$ layers, as well as the $d_{xz,yz}$ orbitals of the Gd$_4$ layer. From $k_{||} \approx \frac{1}{3}(\overline{\text{M}}-\overline{\text{X}})$ counting from the $\overline{\text{M}}$ point and further along the $\overline{\text{M}}-\overline{\text{X}}$ direction, the d_{xz} orbitals of the Rh$_2$ layer start to dominate in the composition of these bands. Within the indicated wave number range the lower band penetrates deeper into the material, where it gains contribution from the Rh$_6$ layer located in the subsurface 4-layer block [blue color in Fig. 2(a)]. The state γ located above the Fermi level is

essentially built by the p_z orbitals of the Si$_1$ layer. While the bands δ have been identified in photoemission experiments performed on Si-terminated (001) surfaces of EuRh$_2$Si$_2$ [20], GdRh$_2$Si$_2$ [21], HoRh$_2$Si$_2$ [36], and YbIr$_2$Si$_2$ [39], the signatures of the γ band have only been seen at the YbIr$_2$Si$_2$(001) surface [39], since in all other measured systems it lies in the conduction band, which is inaccessible to conventional photoemission. Finally, at about -1.4 eV, the η surface state is seen near the $\overline{\text{M}}$ point. Built mainly by $d_{x^2-y^2}$ orbitals and essentially localized in the Rh$_6$ layer, this state plays a pivotal role in the formation of the butterfly-like shape of the Shockley surface state δ (see Sec. III D). Despite abundant photoemission data available on the Si-terminated (001) surface of REX_2Si$_2$, the η state has not been discussed so far.

Figure 2(a) also shows that in spite of the deep-penetrating relaxations some of the bands localized in the second 4-layer block of the Si termination show rather bulk-like behavior. Apart from the blue α and β bands, this is also the case for the resonant band lying within the region of strongly $k_{||}$-dispersive projected states that are crossed by the δ state along $\overline{\text{M}}-\overline{\text{X}}$. These resonant bands are seen in ARPES [36,39] and reflect reasonably the bulk bands' behavior. The latter is because the relaxations in the second 3-layer block are not large and
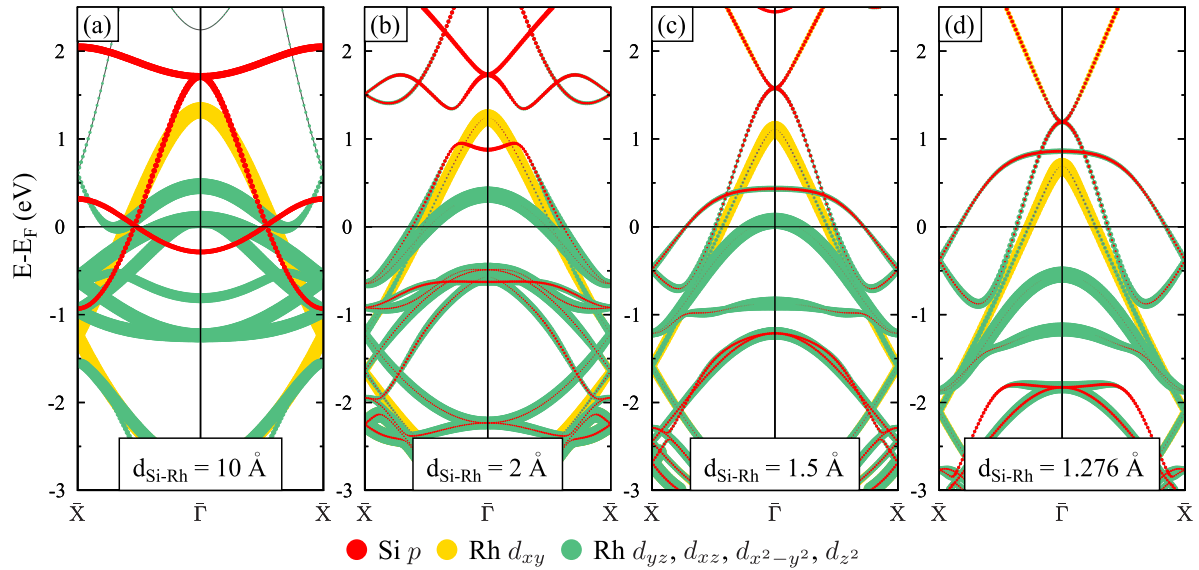
FIG. 3. Electronic band structure of a 3-layer Si-Rh-Si block calculated for different interlayer distances d_{Si-Rh}: (a) $d_{Si-Rh} = 10$ Å, (b) $d_{Si-Rh} = 2$ Å, (c) $d_{Si-Rh} = 1.5$ Å, and (d) $d_{Si-Rh} = 1.276$ Å. The Si p states are shown in red, the Rh d_{xy} in yellow, while all other Rh d states in green. The size of the color circle reflects the contribution of the corresponding state.

the environment of the Rh$_6$ layer, in which these bands are mostly localized, is not very different from that in the bulk. In contrast, the surface states are expectedly strongly affected by relaxations. For example, at the unrelaxed Si termination, the γ band crosses the Fermi level, while the relaxation pushes it completely into the conduction band.

At the Gd termination, the states α and β, formed mainly by the Rh d_{xy} orbitals (Rh$_3$ layer in this case) are also present [Fig. 2(b)]. Their dispersions and energy positions look pretty similar to the corresponding states of the subsurface 4-layer block of the Si termination; cf. Figs. 2(a) and 2(b). There is, however, an appreciable difference between these two cases, consisting in the fact that at the Gd termination the state β is clearly accompanied by another (unlabeled) hole-like state with which it degenerates at the $\overline{\Gamma}$ point at approximately -0.8 eV; at the Si termination this companion state is present as well, although it is much less pronounced. Unlike the Si termination, at the Gd surface there are no Shockley states in the big projected bulk band gap around the $\overline{M}$ point. This fact is used in photoemission experiments on REX_2Si$_2$ for identification of the surface termination after the crystal cleavage. Next, near the $\overline{M}$ point at about -1.4 eV, there is a surface band η. Being of essentially $d_{x^2-y^2}$ character and localized in the Rh$_3$ layer, this state is closely related to the η state seen at the Si termination around the same energies. Finally, in the conduction band there are also 2D states near the $\overline{\Gamma}$ point at about 0.5 eV and the $\overline{X}$ point at approximately 0.4 eV, created mainly by the d_{xy} and the d_{z^2} orbitals of the Gd$_1$ layer, respectively. Since these states are located rather high above the Fermi level we do not discuss their origin in what follows.

Upon inclusion of spin-orbit and magnetic interactions the spin degeneracy of the surface bands is lifted at both Si- and Gd-terminated surfaces; see Fig. 2(c) and Fig. 2(d), respectively. However, the differences between the band structures calculated for the local magnetic moments oriented along the

[110] and [100] directions are insignificant (see Fig. 1 of the Supplemental Material [69]). At the Si-terminated surface, in the vicinity of the $\overline{M}$ point, a complex splitting of the butterfly-like Shockley bands δ is observed, caused by the simultaneous action of the spin-orbit and magnetic interactions [Fig. 2(c)]. In combination with the inversion symmetry breaking near the surface, spin-orbit coupling gives rise to the Bychkov-Rashba effect [70]. The exchange splitting is caused by interaction of the 2D electron states with the ordered Gd $4f$ magnetic moments. Note that the discussed 2D states are predominantly localized either in the surface (orange color) or subsurface (blue color) four-layer block. Therefore, they interact correspondingly with the ferromagnetically ordered Gd$_4$ and Gd$_8$ layers. The latter are stacked antiferromagnetically with respect to each other. For further insight into the interplay of the spin-orbit and magnetic interactions acting on the Shockley bands δ, see Figs. 2 and 3 of the Supplemental Material and their description [69].

C. Electronic structure of the GdRh$_2$Si$_2$(001) thin films

1. Three-layer film

To study the origin of the resonance states in the vicinity of the $\overline{\Gamma}$ point and the surface states near the $\overline{M}$ point, we consider the electronic band structure of paramagnetic GdRh$_2$Si$_2$ thin films, calculated without taking spin-orbit interaction into account. The latter allows us to substantially simplify the derivation of our results and their analysis, without affecting the conclusions drawn in this work. This is because magnetic ordering and spin-orbit interaction are not the fundamental causes of the existence of these states. Indeed, as can be seen from a comparison of Figs. 2(a)–2(b) and Figs. 2(c)–2(d), these interactions only modify surface and resonance states.

As will be shown below, the Rh$_2$Si$_2$ 3-layer block is the minimal structural unit yielding the d_{xy} bands characterized by a linear dispersion in the vicinity of the $\overline{\Gamma}$ point. In the limit

of a semi-infinite crystal, these bands form the continuum of the bulk states, from which the Tamm resonance bands are split off near the Si surface. To prove this statement, we trace the evolution of the Rh_2Si_2 3-layer block electronic structure as a function of the distance between the Si, Rh, and Si layers, that was changed from $d_{Si-Rh} = 10$ Å (noninteracting layers) to the bulk equilibrium distance $d^0_{Si-Rh} = 1.276$ Å. The electronic band structure calculated for the four values of d_{Si-Rh} is presented in Fig. 3. In Fig. 3(a), the situation for $d_{Si-Rh} = 10$ Å is illustrated. In this case, the band structure is a superposition of the band structures of the freestanding Rh and Si layers. The Si and Rh layers have a simple square and square base-centered lattices, respectively. These symmetries determine the band structure of the Rh and Si layers seen in Fig. 3(a). Within each Si layer, the bonds between atoms are formed by the overlapping p_x and p_y orbitals directed toward the nearest neighbors. In Fig. 3(a), the low-energy electronic structure of a Si layer is represented by three bands, two of which have a weak dispersion along the $\overline{\Gamma}$–$\overline{X}$ direction (with band widths of about 0.37 and 0.63 eV), while the third band disperses over a larger energy range of approximately 2.6 eV. The narrow band near the Fermi level is built by the p_z orbitals. The other two bands are formed by the p_x and p_y orbitals: along the $(0, 0)$–$(\frac{\pi}{a}, 0)$ $[(0, 0)$–$(0, \frac{\pi}{a})]$ direction, the flat band around 2 eV is built by Si p_y (p_x) orbitals, while the band characterized by notable dispersion is built up by p_x (p_y) orbitals. In the Rh layer, the d_{xy} orbitals directed along the Rh-Rh bonds form the covalent component of the interatomic forces, while the remaining d orbitals create the metallic component. Hybridization of the d_{xy} orbitals within the Rh layer gives rise to a strongly dispersive hole-like band of d_{xy} symmetry (shown in yellow in Fig. 3). The reduction of the interlayer spacings d_{Si-Rh} [Figs. 3(b) and 3(c)] shifts most of the Rh d states to lower energies, while the dispersion of the hole-like d_{xy} band crossing the Fermi level becomes almost linear. Figure 3 also illustrates the Si p and Rh d orbital hybridization upon the approach of the Si and Rh layers. Due to this hybridization, Si p_x, p_y and Rh d_{xy} orbitals form an electron-like band lying above 1 eV and showing a linear dispersion in a considerable wave-vector interval [Fig. 3(d)]. Thus, precursors of the resonance states near the $\overline{\Gamma}$ point having almost linear dispersion are already formed in the Si-Rh-Si 3-layer block. However, both the dispersion and orbital composition of the electron-like band as well as its energy separation from the hole-like band are still significantly different from those seen at Si or Gd terminations of the the $GdRh_2Si_2$ surface. As is shown in the next section, addition of the Gd layer to the Rh_2Si_2 block makes these bands resemble closely the resonant states near the $\overline{\Gamma}$ point.

2. Four-layer film

The addition of a Gd atomic layer to the Si-Rh-Si block leads to the formation of a stoichiometric $GdRh_2Si_2(001)$ film of minimal thickness. To consider the formation of the 4-layer film electronic structure we performed calculations for different distances between the Si-Rh-Si block and the Gd atomic layer. The distance was varied from $d_{3L-Gd} = 10$ Å to the bulk equilibrium distance $d^0_{3L-Gd} = 1.243$ Å. Figure 4 shows the band structure of such a system for six different

values of d_{3L-Gd}. When the distance between the Rh_2Si_2 and Gd layers is equal to 10 Å [Fig. 4(a)], the spectrum represents a superposition of the band structures of the 3-layer block [Fig. 3(d)] and a freestanding Gd monolayer. As was shown above, in the band spectrum of the freestanding 3-layer block [Fig. 3(d)], a pair of electron- and hole-like linear bands is observed, labeled in Fig. 4 as α and β, respectively. Note that the bands α and α^* are fourfold degenerate at the $\overline{\Gamma}$ point due to the crystal symmetry. Above -0.6 eV, the d bands dominate in the Gd layer electronic structure (highlighted in blue). Only the band observed along all considered symmetry directions and coming to the $\overline{X}$ point at -1.2 eV has essentially s character. A significant hybridization between the two subsystems starts at about 5 Å, which is manifested by a lifting of the fourfold degeneracies along the $\overline{X}$–$\overline{M}$–$\overline{X}$ direction and the appearance of avoided crossings due to interaction between the Gd- and Rh_2Si_2-derived bands.

Let us now trace the evolution of the band structure upon further gradual approaching of the layers. When reducing d_{3L-Gd} to 3 Å [Figs. 4(b)–4(d)], the band α becomes more linear and the point of its fourfold degeneracy with the band α^* shifts toward the Fermi level. The latter leads to a decrease of the energy gap between the degeneracy point and the maximum of the band β. Below 3 Å, this gap reduction starts being accompanied by a gradual increase of the Rh d_{xy} contribution to the band α. At about 2 Å, the gap disappears and the bands β, α, and α^* become accidentally degenerate [Fig. 4(e)]. Further approaching [Fig. 4(f)] leads to the re-opening and subsequent increase of this gap, as well as to a parabolization of the bands α and β in the vicinity of the $\overline{\Gamma}$ point. After the gap reopening the fourfold degeneracy is observed for the bands β and α^*, both of them featuring a noticeable contribution of Si p states near the $\overline{\Gamma}$ point, which were not originally present in the band β. At the same time the Si p contribution to the band α at and near the $\overline{\Gamma}$ point is almost gone. The described modification of the bands near the $\overline{\Gamma}$ point, which is somewhat similar to a band gap inversion, results in a formation of the electron-like d_{xy} band, whose dispersion resembles closely that of the upper part of the resonance state residing at the Gd-terminated $GdRh_2Si_2(001)$ surface [Fig. 2(b)].

At $d^0_{3L-Gd} = 1.243$ Å (the bulk equilibrium distance), the band β appears to lie below the Fermi level, while the band α remains unoccupied. As can be seen in Fig. 4, reduction of the distance between the 3-layer block and the Gd atomic layer causes a significant hybridization of Gd, Rh, and Si electronic states and, thus, the modification of the electronic structure. In particular, the electronic states of the 3-layer block are shifted to lower energies, whereas the Gd states are shifted to higher energies. This is due to a charge transfer of $\simeq 1.27$ electrons per cell from the Gd atoms to the 3-layer Si-Rh-Si block.

In contrast to the states in the vicinity of the $\overline{\Gamma}$ point, those near the $\overline{M}$ point experience more dramatic changes during the approach of the 3-layer block and the Gd layer. Let us consider the bands labeled as γ and δ in Fig. 4, whose hybridization will define the band dispersion of the 4-layer near the $\overline{M}$ point. As can be seen in Fig. 4(a) ($d_{3L-Gd} = 10$ Å), the band δ, localized in the Si-Rh-Si block, is built mainly by Si p orbitals, while the band γ is formed by Gd d orbitals. As the two subsystems approach each other,
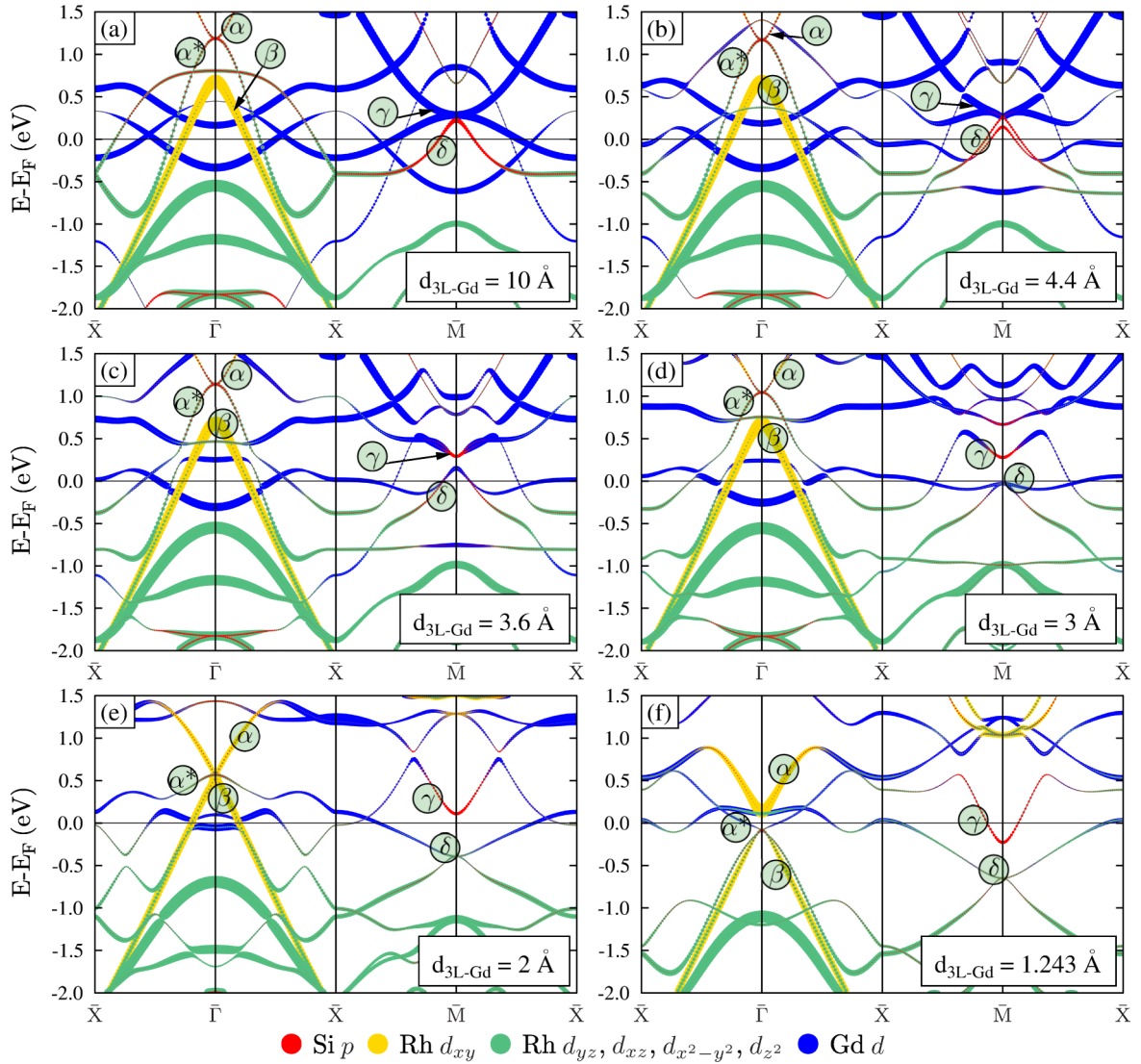
FIG. 4. Electronic band structure of the 4-layer $GdRh_2Si_2(001)$ film calculated for different distances d_{3L-Gd} between the 3-layer Si-Rh-Si block and the Gd layer: (a) $d_{3L-Gd} = 10$ Å, (b) $d_{3L-Gd} = 4.4$ Å, (c) $d_{3L-Gd} = 3.6$ Å, (d) $d_{3L-Gd} = 3$ Å, (e) $d_{3L-Gd} = 2$ Å, (f) $d_{3L-Gd} = 1.243$ Å. The Si p states are shown in red, the Rh d_{xy} in yellow, all other Rh d in green, and Gd d in blue. The size of the color circle reflects the contribution of the corresponding state.

these bands get significantly modified due to the increasing hybridization between the layers [Fig. 4(b)]. In particular, this hybridization results in the inversion of the bands γ and δ. Indeed, while at 4.4 Å the bands δ (γ) are formed by Si p (Gd d) orbitals, at about 3.9 Å they start to be predominantly composed of Gd d (Si p) states in the close vicinity of the $\overline{M}$ point; further reduction of d_{3L-Gd} results in the situation shown in Fig. 4(c). Next, when the subsystems come closer to each other, the Rh contribution to the band δ increases gradually at the expense of the Gd contribution [Figs. 4(c)–4(f)], which is due to the above mentioned charge transfer from the Gd layer to the 3-layer Si-Rh-Si block. In Fig. 4(f), three bands can be seen in the energy range from −1.0 to 0.5 eV. The two bands, that are degenerate at the $\overline{M}$ point (labeled by δ) are built essentially by the Rh $d_{x^2-y^2}$ orbitals, while the band descending from the unoccupied part of the spectrum (labeled by γ) is built mainly by the Si p orbitals. These bands represent themselves precursors of the Shockley

surface states observed at the Si-terminated $GdRh_2Si_2(001)$ surface near the $\overline{M}$ point. Indeed, by comparing Figs. 2(a) and 4(f) one can clearly see significant similarities of the bands δ and γ to the surface states localized in the topmost Si-terminated 4-layer block of the 32-layer paramagnetic film in the vicinity of the $\overline{M}$ point. However, in the 4-layer-thick film these bands lie approximately 0.2–0.4 eV lower in energy than those at the surface of the 32-layer film. Our calculations show that this difference in the energy position is caused by significant relaxation of the Si-terminated surface, which was analyzed in Sec. III A. Qualitatively, there is still a noticeable difference between the dispersions of the 4- and 32-layer films along the $\overline{X}$–$\overline{M}$ direction: in the latter case, the hole-like band of the occupied surface state changes its character to an electron-like one at approximately $\frac{1}{3}(\overline{X}-\overline{M})$. The formation of such a dispersion requires further increase of the $GdRh_2Si_2(001)$ film thickness, as is discussed in the next section.
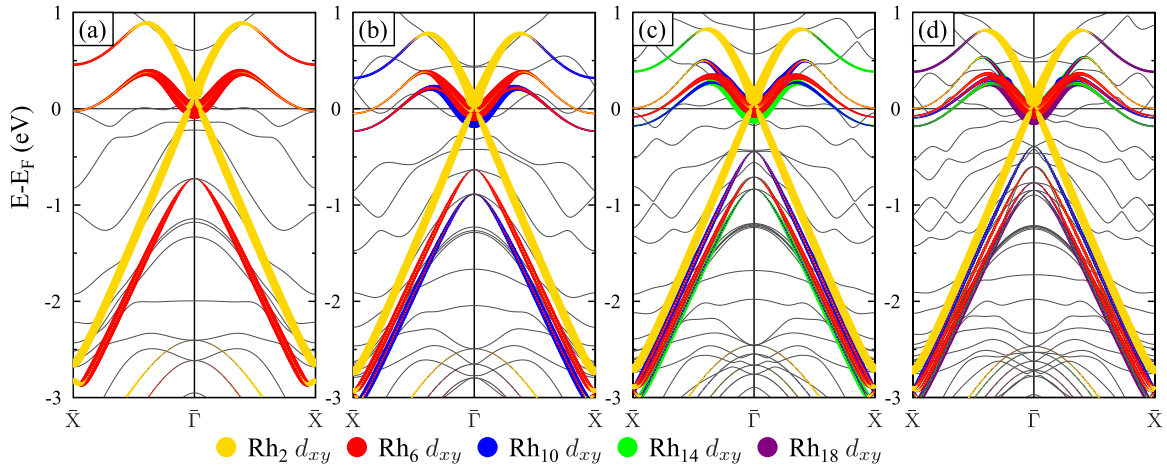
FIG. 5. Electronic band structure of stoichiometric GdRh$_2$Si$_2$(001) films with thicknesses of 8 (a), 12 (b), 16 (c), and 20 (d) layers calculated along the $\overline{\text{X}}$–$\overline{\Gamma}$–$\overline{\text{X}}$ direction in the SBZ. The contributions of the Rh d_{xy} states from the 2nd, 6th, 10th, 14th, and 18th layer (numbered from the Si surface) are shown in yellow, red, blue, green and purple, respectively. The size of the color circle reflects the contribution of the corresponding state.

D. *N*-layer films (*N* = 8, 12, 16, 20): Thickness dependence of the electronic structure

Let us now consider the evolution of the band structure of the stoichiometric films upon the increase of their thickness. For the $\overline{\text{X}}$–$\overline{\Gamma}$–$\overline{\text{X}}$ direction this evolution is illustrated in Fig. 5. The electronic structure of the 8-layer film (two 4-layer blocks) reveals two sets of Rh d_{xy} bands, that are highlighted in yellow and red in Fig. 5(a). The bands shown in yellow are localized near the Si-terminated surface of the film and lie in energy above the bands highlighted in red, which are localized near the Gd-terminated surface. Such an energy location of these bands is caused by a transfer of approximately $\simeq 0.8e$ from the 4-layer Si-terminated block to the 4-layer Gd-terminated block. This leads to a shift of the Rh d_{xy} states localized in the Gd-terminated (Si-terminated) block to lower (higher) energies.

Note that the electron- and hole-like d_{xy} bands near the $\overline{\Gamma}$ point at the Gd surface are separated by a gap of approximately 0.8 eV, while at the Si surface they approach each other much closer. Apart from the different environments of the corresponding Rh$_2$Si$_2$ blocks, this also should be related to the relaxations, that yield significantly different values of both $d_{\text{3L}-\text{Gd}}$ and $d_{\text{Si}-\text{Rh}}$ in the two blocks. First, in the Si-terminated block of the 8-layer film $d_{\text{3L}-\text{Gd}}$ increases with respect to the bulk equilibrium distance $d_{\text{3L}-\text{Gd}}^0$ (1.348 vs 1.243 Å), which is accompanied by (i) a linearization of both the electron- and hole-like Rh d_{xy} bands and (ii) a decrease of the gap between them. This is similar to what happens in the 4-layer film when $d_{\text{3L}-\text{Gd}}$ increases from 1.243 to 2 Å [cf. Fig. 4(f) and Fig. 4(e)]. In the Gd-terminated block, $d_{\text{3L}-\text{Gd}}$ decreases upon relaxation (0.882 vs 1.243 Å), which, on the contrary, leads to (i) a partial recovery of the quadratic dispersion of both the electron- and hole-like Rh d_{xy} bands and (ii) an increase of the gap between them. Second, in the Si-terminated block, the Si-Rh-Si 3-layer is compressed upon relaxation as compared to the bulk (i.e., both $d_{\text{Si}-\text{Rh}}$ spacings decrease: 1.175 and 1.223 Å vs 1.276 Å), contributing to the linearization of the Rh d_{xy} bands localized in this block. A similar picture can

be seen in the electronic spectrum of the 3-layer film upon decreasing $d_{\text{Si}-\text{Rh}}$ from 1.5 to 1.276 Å [cf. Fig. 3(c) and Fig. 3(d)]. In contrast, the expansion of the Si-Rh-Si 3-layer of the Gd-terminated block due to relaxation (1.366 and 1.333 Å vs 1.276 Å) makes the respective band more parabolic near the $\overline{\Gamma}$ point.

Upon increasing the film thickness from 8 to 12, 16, and 20 atomic layers, i.e., from 2 to 3, 4, and 5 GdRh$_2$Si$_2$ 4-layer blocks, the number of bands built by the Rh d_{xy} orbitals in the films' spectra increases in accordance with the number of 4-layer blocks [Figs. 5(b)–5(d)]. At a thickness of 20 layers a significant hybridization between the d_{xy} bands localized in the inner 4-layer blocks is clearly seen [Fig. 5(d)]. Further increase of the film thickness up to the semi-infinite crystal limit leads to the formation of a well-defined continuum of bulk Rh d_{xy} states [Figs. 2(a), 2(b)]. At the Si termination of the semi-infinite crystal the resonance states split off from this bulk continuum (upward in energy) while maintaining the dispersion and orbital composition of those bulk states, which proves that these two-dimensional states appear via the Tamm mechanism. Note that the d_{xy} orbitals of the Rh layers closest to the Si- and Gd-terminated surfaces contribute as well to the bands built mainly by d_{xy} orbitals of the deeper-lying Rh layers. For example, for the 20-layer film at $k_{||} = \frac{1}{4}(\overline{\Gamma}–\overline{\text{X}})$ this contribution is equal to 8% for the Rh$_2$ layer (subsurface layer of the Si termination), while for the Rh$_{18}$ (third layer at the Gd termination) it reaches 30%. This indicates penetration of the wave function of the subsurface Rh states into the bulk and proves their resonance character in agreement with results reported in Ref. [21].

Let us now trace the evolution of the two-dimensional electronic states in the vicinity of the $\overline{\text{M}}$ point upon increasing the film thickness. The film thickness increase from the 4-layer [Fig. 4(f)] to the 8-layer [Fig. 6(a)] is accompanied by a doubling of the number of electronic bands in the film spectrum and, in particular, leads to two sets of Rh-derived bands within a 1.5 eV interval below the Fermi level [marked as δ and η in Fig. 6(a)]. Both pairs of bands, δ and η, show a
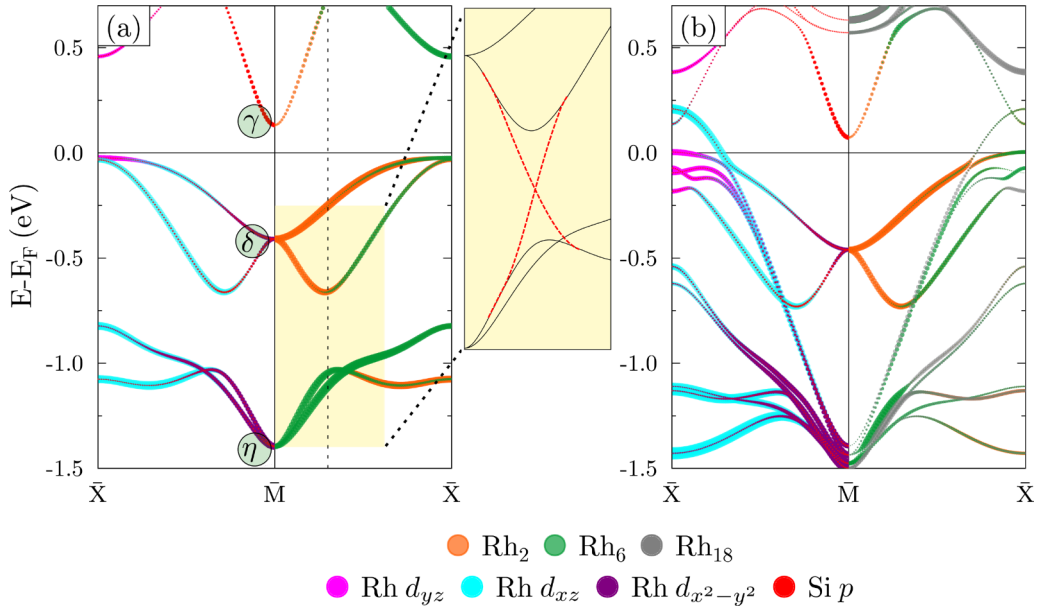
FIG. 6. Electronic band structure of the GdRh$_2$Si$_2$(001) films with thicknesses of 8 (a) and 20 (b) layers calculated along the $\overline{X}$–$\overline{M}$–$\overline{X}$ direction in the SBZ. On the left-hand sides of panels (a) and (b) the contributions of the d_{yz}, d_{xz}, $d_{x^2-y^2}$ states of all Rh layers as well as those of the p states of all Si layers are shown in magenta, cyan, purple, and red circles, respectively. On the right-hand sides, the Rh d_{xy} state contributions of the 2nd, 6th, and 18th Rh layers (numbered from the Si surface) are shown in orange, green, and gray, respectively. The Rh d_{xy} state contributions of the 10th and 14th Rh layers are not shown. The inset to (a) illustrates the avoided crossing arising due to interaction of the δ and η bands. The size of the color circle reflects the contribution of the corresponding state.

characteristic fourfold degeneracy at the $\overline{M}$ point and a similar orbital composition ($d_{x^2-y^2}$ near the $\overline{M}$ point, which gradually changes into a d_{xz} symmetry further along the $\overline{M}$–$\overline{X}$ direction). However, the dispersions of the two pairs of bands differ significantly. Apart from the differences in environments of the Rh layers in the two blocks that affect the dispersion of the corresponding bands, there is another important factor that governs their dispersion, which is the interaction between them. In fact, it is the hybridization between the bands originating from the different 4-layer blocks that gives rise to the butterfly-like dispersion of the bands marked as δ. Indeed, while the lower band of δ is exclusively localized in the Si-terminated block near the $\overline{M}$ point, it becomes shared between the two blocks starting from $k_{||} \approx \frac{1}{3}(\overline{M}$–$\overline{X})$ (shown by the vertical black dashed line), where its group velocity changes sign Fig. 6(a). The upper band of η shows a somewhat similar behavior, residing in the Gd-terminated block near the $\overline{M}$ point but relocating to a large extent to another block starting from the same $k_{||}$, where the sign of the group velocity changes as well. In other words, the hole-like band of the Si-terminated block interacts with the electron-like band of the Gd-terminated block as a result of which the avoided crossing appears at $k_{||} \approx \frac{1}{3}(\overline{M}$–$\overline{X})$, as is illustrated in the inset of Fig. 6(a). Thus, the butterfly-shaped surface state of the 32-layer GdRh$_2$Si$_2$ film [Fig. 2(a)] is formed already at a thickness of 8 layers. Finally, as far as the unoccupied states are concerned, comparing Figs. 2(a) and 6(a), it can be seen that the γ band is completely formed in the 8-layer film and resides at almost the same energy, which is caused by similar relaxations near the Si termination of the 8- and 32-layer films.

Figure 6(b) shows the band structure of the 20-layer film. As compared to the spectrum of the 8-layer film, one can see three additional pairs of bands whose origin and orbital composition are similar to those of δ and η. However, in contrast to the latter, these new bands, being localized in the internal blocks of the film, have a dispersion characteristic of the bulk states seen along the $\overline{M}$–$\overline{X}$ direction [cf. Figs. 2(a), 2(b)]. In particular, there is a group of closely packed $k_{||}$-dispersive bands that go through the butterfly-like state without significant interaction. At the (001) surface of the semi-infinite crystal they form the continuum of the bulk projected bands with a weak k_z dispersion that separate the two local projected bulk band gaps in which the state δ is located at the Si termination [Fig. 2(a)]. The part of the butterfly-like state located in the larger band gap localizes in real space in the topmost 4 layers of the Si surface, while the part located in the smaller gap appears to be shared between the first and second blocks of the Si-terminated surface. Unlike the 8-layer film, there are two bands of the type η that have markedly two-dimensional character near $\overline{M}$: one of them is located in the subsurface 4-layer block of the Si termination (shown in green); the other one resides in the surface block of the Gd termination [shown in gray; cf. also Figs. 2(a), 2(b)]. Upon approaching the $\overline{M}$ point these bands become resonant, entering the continuum of the bulk states [Figs. 2(a), 2(b)]. However, the inclusion of the spin-orbit interaction opens a local band gap in the projected bands at the $\overline{M}$ point around an energy of -1.4 eV [Figs. 2(c), 2(d)]. Due to this, the bands η of both terminations acquire purely surface character, being now located inside the local projected band gap.

IV. CONCLUSION

The origin of the two-dimensional electronic states at the (001) surface of GdRh$_2$Si$_2$ has been studied using first-principles calculations. Two surface terminations, Si and Gd, reported in recent experimental studies have been considered, and the differences of their electronic structures have been analyzed in detail.

Both the Si and Gd surfaces reveal strong structural relaxations that penetrate relatively deeply into the material. While the surface states are expectedly affected by the relaxations, the subsurface 2D states are not shifted to local or symmetry gaps upon relaxation and follow closely the projected bulk bands' behavior. This circumstance allows using such bands as a reliable reference in the identification of bulk bands in ultraviolet ARPES measurements, that probe only the near surface region.

It has been found that the resonance state, located around the $\overline{\Gamma}$ point and observed in several photoemission experiments, in the case of Si termination is formed via the Tamm mechanism. The latter means that this state is split off from the projected bulk states of similar dispersion and the same orbital character into a continuum symmetry gap where it coexists with degenerate projected bulk states of different symmetry. In contrast, the resonant state at the Gd termination does not come out from the projected band region and is hybridized with the bulk states much more strongly. The differences between the resonance states at the Si- and Gd-terminated surfaces arise due to the different relaxations near these surfaces.

The precursors of the Shockley surface states, located in the projected band gap around the $\overline{M}$ point at the Si-terminated GdRh$_2$Si$_2$(001) surface, are formed already in a stoichiometric film of minimal thickness (4 layers). Further, we have shown that the butterfly-like dispersion of the valence band surface state arises in the 8-layer-thick film due to hybridization between the two bands' precursors, that come from the two different 4-layer blocks (Si- and Gd-terminated). Because

of this hybridization, the butterfly-shaped Shockley state in real space is shared between the subsurface and surface 4-layer blocks. Further increase of the thickness from 8 layers to the semi-infinite medium limit only leads to slight changes of the energy positions of these states.

All these results have been obtained without taking spin-orbit and magnetic interactions into account, since they are not the fundamental causes of the existence of these states. Inclusion of these interactions in the calculation lifts the spin degeneracy of the surface bands thus modifying their dispersion. However, the differences between the band structures calculated for the Gd $4f$ moments oriented along the [110] and [100] directions appear to be subtle.

Thus, our study sheds light on the origin of the two-dimensional electronic states at the GdRh$_2$Si$_2$(001) surface and explains their dispersion seen in angle-resolved photoemission spectroscopy experiments. Similar formation mechanisms of the surface and resonance states should be expected in a wide class of the REX_2Si$_2$ compounds.

[1] F. Steglich, J. Aarts, C. D. Bredl, W. Lieke, D. Meschede, W. Franz, and H. Schäfer, Phys. Rev. Lett. **43**, 1892 (1979).

[2] O. Trovarelli, C. Geibel, S. Mederle, C. Langhammer, F. M. Grosche, P. Gegenwart, M. Lang, G. Sparn, and F. Steglich, Phys. Rev. Lett. **85**, 626 (2000).

[3] P. Gegenwart, J. Custers, C. Geibel, K. Neumaier, T. Tayama, K. Tenya, O. Trovarelli, and F. Steglich, Phys. Rev. Lett. **89**, 056402 (2002).

[4] J. Custers, P. Gegenwart, H. Wilhelm, K. Neumaier, Y. Tokiwa, O. Trovarelli, C. Geibel, F. Steglich, C. Pepin, and P. Coleman, Nature (London) **424**, 524 (2003).

[5] J. Sichelschmidt, V. A. Ivanshin, J. Ferstl, C. Geibel, and F. Steglich, Phys. Rev. Lett. **91**, 156401 (2003).

[6] P. Coleman and A. J. Schofield, Nature (London) **433**, 226 (2005).

[7] N. D. Mathur, F. M. Grosche, S. R. Julian, I. R. Walker, D. M. Freye, R. K. W. Haselwimmer, and G. G. Lonzarich, Nature (London) **394**, 39 (1998).

[8] S. S. Saxena, P. Agarwal, K. Ahilan, F. M. Grosche, R. K. W. Haselwimmer, M. J. Steiner, E. Pugh, I. R. Walker, S. R. Julian, P. Monthoux, G. G. Lonzarich, A. Huxley, I. Sheikin, D. Braithwaite, and J. Flouquet, Nature (London) **406**, 587 (2000).

[9] O. Stockert, E. Faulhaber, G. Zwicknagl, N. Stüßer, H. S. Jeevan, M. Deppe, R. Borth, R. Küchler, M. Loewenhaupt, C. Geibel, and F. Steglich, Phys. Rev. Lett. **92**, 136401 (2004).

[10] H. von Löhneysen, J. Phys.: Condens. Matter **8**, 9689 (1996).

[11] H. v. Löhneysen, T. Pietrus, G. Portisch, H. G. Schlager, A. Schröder, M. Sieck, and T. Trappmann, Phys. Rev. Lett. **72**, 3262 (1994).

[12] P. Gegenwart, Q. Si, and F. Steglich, Nat. Phys. **4**, 186 (2008).

[13] D. M. Broun, Nat. Phys. **4**, 170 (2008).

[14] P. C. Canfield, Nat. Phys. **4**, 167 (2008).

[15] P. Gegenwart, T. Westerkamp, C. Krellner, Y. Tokiwa, S. Paschen, C. Geibel, F. Steglich, E. Abrahams, and Q. Si, Science **315**, 969 (2007).

[16] R. Küchler, N. Oeschler, P. Gegenwart, T. Cichorek, K. Neumaier, O. Tegus, C. Geibel, J. A. Mydosh, F. Steglich, L. Zhu, and Q. Si, Phys. Rev. Lett. **91**, 066405 (2003).

[17] K. Ishida, K. Okamoto, Y. Kawasaki, Y. Kitaoka, O. Trovarelli, C. Geibel, and F. Steglich, Phys. Rev. Lett. **89**, 107202 (2002).

[18] K. Ishida, D. E. MacLaughlin, B.-L. Young, K. Okamoto, Y. Kawasaki, Y. Kitaoka, G. J. Nieuwenhuys, R. H. Heffner, O. O. Bernal, W. Higemoto, A. Koda, R. Kadono, O. Trovarelli, C. Geibel, and F. Steglich, Phys. Rev. B **68**, 184401 (2003).

[19] D. Gignoux and D. Schmitt, in *Handbook of Magnetic Materials* (Elsevier, Amsterdam, 1997), Vol. 10, pp. 239–413.

[20] A. Chikina, M. Höppner, S. Seiro, K. Kummer, S. Danzenbächer, S. Patil, A. Generalov, M. Güttler, Yu. Kucherenko, E. V. Chulkov, Yu. M. Koroteev, K. Koepernik, C. Geibel, M. Shi, M. Radovic, C. Laubschat, and D. V. Vyalikh, Nat. Commun. **5**, 3171 (2014).

[21] M. Güttler, A. Generalov, M. M. Otrokov, K. Kummer, K. Kliemt, A. Fedorov, A. Chikina, S. Danzenbächer, S. Schulz, E. V. Chulkov, Yu. M. Koroteev, N. Caroca-Canales, M. Shi, M. Radovic, C. Geibel, C. Laubschat, P. Dudin, T. K. Kim, M. Hoesch, C. Krellner, and D. V. Vyalikh, Sci. Rep. **6**, 24254 (2016).

[22] S. Friedemann, T. Westerkamp, M. Brando, N. Oeschler, S. Wirth, P. Gegenwart, C. Krellner, C. Geibel, and F. Steglich, Nat. Phys. **5**, 465 (2009).

[23] S. Ernst, S. Kirchner, C. Krellner, C. Geibel, G. Zwicknagl, F. Steglich, and S. Wirth, Nature (London) **474**, 362 (2011).

[24] E. Schuberth, M. Tippmann, L. Steinke, S. Lausberg, A. Steppke, M. Brando, C. Krellner, C. Geibel, R. Yu, Q. Si, and F. Steglich, Science **351**, 485 (2016).

[25] S. Friedemann, N. Oeschler, S. Wirth, C. Krellner, C. Geibel, F. Steglich, S. Paschen, S. Kirchner, and Q. Si, Proc. Natl. Acad. Sci. USA **107**, 14547 (2010).

[26] H. Pfau, S. Hartmann, U. Stockert, P. Sun, S. Lausberg, M. Brando, S. Friedemann, C. Krellner, C. Geibel, S. Wirth, S. Kirchner, E. Abrahams, Q. Si, and F. Steglich, Nature (London) **484**, 493 (2012).

[27] A. Chikina, A. Generalov, K. Kummer, M. Güttler, V. N. Antonov, Yu. Kucherenko, K. Kliemt, C. Krellner, S. Danzenbächer, T. Kim, P. Dudin, C. Geibel, C. Laubschat, and D. V. Vyalikh, Phys. Rev. B **95**, 155127 (2017).

[28] J. Sichelschmidt, S. Kimura, C. Krellner, C. Geibel, and F. Steglich, Physica B (Amsterdam) **403**, 775 (2008).

[29] K. Kaneko, O. Stockert, N. Mufti, K. Kiefer, C. Klingner, C. Krellner, C. Geibel, and F. Steglich, J. Phys.: Conf. Ser. **200**, 032031 (2010).

[30] Q. Si and F. Steglich, Science **329**, 1161 (2010).

[31] P. M. C. Rourke, A. McCollam, G. Lapertot, G. Knebel, J. Flouquet, and S. R. Julian, Phys. Rev. Lett. **101**, 237205 (2008).

[32] Y.-F. Yang and D. Pines, Proc. Natl. Acad. Sci. USA **111**, 8398 (2014).

[33] E. Abrahams and P. Wölfle, Proc. Natl. Acad. Sci. USA **109**, 3238 (2012).

[34] K. Kummer, C. Geibel, C. Krellner, G. Zwicknagl, C. Laubschat, N. B. Brookes, and D. V. Vyalikh, Nat. Commun. **9**, 2011 (2018).

[35] S. Schulz, I. A. Nechaev, M. Güttler, G. Poelchen, A. Generalov, S. Danzenbächer, A. Chikina, S. Seiro, K. Kliemt, A. Yu. Vyazovskaya, T. K. Kim, P. Dudin, E. V. Chulkov,

[36] C. Laubschat, E. E. Krasovskii, C. Geibel, C. Krellner, K. Kummer, and D. V. Vyalikh, npj Quantum Mater. **4**, 26 (2019).

[37] A. Generalov, M. M. Otrokov, A. Chikina, K. Kliemt, K. Kummer, M. Höppner, M. Güttler, S. Seiro, A. Fedorov, S. Schulz, S. Danzenbächer, E. V. Chulkov, C. Geibel, C. Laubschat, P. Dudin, M. Hoesch, T. Kim, M. Radovic, M. Shi, N. C. Plumb, C. Krellner, and D. V. Vyalikh, Nano Lett. **17**, 811 (2017).

[38] M. Güttler, K. Kummer, S. Patil, M. Höppner, A. Hannaske, S. Danzenbächer, M. Shi, M. Radovic, E. Rienks, C. Laubschat, C. Geibel, and D. V. Vyalikh, Phys. Rev. B **90**, 195138 (2014).

[39] M. Höppner, S. Seiro, A. Chikina, A. Fedorov, M. Güttler, S. Danzenbächer, A. Generalov, K. Kummer, S. Patil, S. L. Molodtsov, Y. Kucherenko, C. Geibel, V. N. Strocov, M. Shi, M. Radovic, T. Schmitt, C. Laubschat, and D. V. Vyalikh, Nat. Commun. **4**, 1646 (2013).

[40] A. Generalov, J. Falke, I. A. Nechaev, M. M. Otrokov, M. Güttler, A. Chikina, K. Kliemt, S. Seiro, K. Kummer, S. Danzenbächer, D. Usachov, T. K. Kim, P. Dudin, E. V. Chulkov, C. Laubschat, C. Geibel, C. Krellner, and D. V. Vyalikh, Phys. Rev. B **98**, 115157 (2018).

[41] D. V. Vyalikh, S. Danzenbächer, Yu. Kucherenko, C. Krellner, C. Geibel, C. Laubschat, M. Shi, L. Patthey, R. Follath, and S. L. Molodtsov, Phys. Rev. Lett. **103**, 137601 (2009).

[42] S. Danzenbächer, D. V. Vyalikh, K. Kummer, C. Krellner, M. Holder, M. Höppner, Yu. Kucherenko, C. Geibel, M. Shi, L. Patthey, S. L. Molodtsov, and C. Laubschat, Phys. Rev. Lett. **107**, 267601 (2011).

[43] K. Kummer, S. Patil, A. Chikina, M. Güttler, M. Höppner, A. Generalov, S. Danzenbächer, S. Seiro, A. Hannaske, C. Krellner, Yu. Kucherenko, M. Shi, M. Radovic, E. Rienks, G. Zwicknagl, K. Matho, J. W. Allen, C. Laubschat, C. Geibel, and D. V. Vyalikh, Phys. Rev. X **5**, 011028 (2015).

[44] A. F. Santander-Syro, M. Klein, F. L. Boariu, A. Nuber, P. Lejay, and F. Reinert, Nat. Phys. **5**, 637 (2009).

[45] W. Shockley, Phys. Rev. **56**, 317 (1939).

[46] S. G. Davison and M. Stęślicka, *Basic Theory of Surface States* (Oxford University Press, Oxford, 1992).

[47] M. Hoesch, M. Muntwiler, V. N. Petrov, M. Hengsberger, L. Patthey, M. Shi, M. Falub, T. Greber, and J. Osterwalder, Phys. Rev. B **69**, 241401(R) (2004).

[48] E. V. Chulkov, V. M. Silkin, and M. Machado, Surf. Sci. **482–485**, 693 (2001).

[49] A. Nuber, M. Higashiguchi, F. Forster, P. Blaha, K. Shimada, and F. Reinert, Phys. Rev. B **78**, 195412 (2008).

[50] J. Jiang, S. S. Tsirkin, K. Shimada, H. Iwasawa, M. Arita, H. Anzai, H. Namatame, M. Taniguchi, I. Yu. Sklyadneva, R. Heid, K.-P. Bohnen, P. M. Echenique, and E. V. Chulkov, Phys. Rev. B **89**, 085404 (2014).

[51] R. A. Bartynski, E. Jensen, T. Gustafsson, and E. W. Plummer, Phys. Rev. B **32**, 1921 (1985).

[52] E. V. Chulkov, V. M. Silkin, and E. N. Shirykalov, Surf. Sci. **188**, 287 (1987).

[53] S. N. Molotkov, JETP Lett. **90**, 339 (2009).

[54] I. Tamm, Z. Phys. **76**, 849 (1932).

[55] A. Szytuła, A. Budkowski, M. Ślaski, and R. Zach, Solid State Commun. **57**, 813 (1986).

[56] A. Szytuła and J. Leciejewicz, in *Handbook on the Physics and Chemistry of Rare Earths* (Elsevier, Amsterdam, 1989), Vol. 12, pp. 133–211.

[56] K. Kliemt and C. Krellner, J. Cryst. Growth **419**, 37 (2015).

[57] K. Kliemt, M. Hofmann-Kliemt, K. Kummer, F. Yakhou-Harris, C. Krellner, and C. Geibel, Phys. Rev. B **95**, 134403 (2017).

[58] P. E. Blöchl, Phys. Rev. B **50**, 17953 (1994).

[59] G. Kresse and J. Furthmüller, Phys. Rev. B **54**, 11169 (1996).

[60] G. Kresse and D. Joubert, Phys. Rev. B **59**, 1758 (1999).

[61] E. Wimmer, H. Krakauer, M. Weinert, and A. J. Freeman, Phys. Rev. B **24**, 864 (1981).

[62] FLEUR site, http://www.flapw.de.

[63] J. P. Perdew, K. Burke, and M. Ernzerhof, Phys. Rev. Lett. **77**, 3865 (1996).

[64] D. Koelling and B. Harmon, J. Phys. C: Solid State Phys. **10**, 3107 (1977).

[65] V. I. Anisimov, J. Zaanen, and O. K. Andersen, Phys. Rev. B **44**, 943 (1991).

[66] S. L. Dudarev, G. A. Botton, S. Y. Savrasov, C. J. Humphreys, and A. P. Sutton, Phys. Rev. B **57**, 1505 (1998).

[67] G. Henkelman, A. Arnaldsson, and H. Jónsson, Comput. Mater. Sci. **36**, 354 (2006).

[68] I. M. Lifshitz and S. I. Pekar, Usp. Fiz. Nauk **56**, 531 (1955).

[69] See Supplemental Material at http://link.aps.org/supplemental/10.1103/PhysRevB.100.075140 for a detailed description of surface band structure of GdRh$_2$Si$_2$(001) calculated along the high-symmetry directions of the surface Brillouin zone for the Si- and Gd-terminated surfaces and Gd 4f moments oriented along the [100] and [110] directions.

[70] Yu. A. Bychkov and E. I. Rashba, JETP Lett. **39**, 78 (1984).